Published in final edited form as:
Circ Res. 2010 December 10; 107(12): 1503–1511. doi:10.1161/CIRCRESAHA.110.232470.

A Major Role for hERG in Determining Frequency of Reentry in Neonatal Rat Ventricular Myocyte Monolayer

Luqia Hou, MS[1,2,*], **Makarand Deo, PhD**[1,*], **Philip Furspan, PhD**[1], **Sandeep V. Pandit, PhD**[1], **Sergey Mironov, PhD**[1], **David S Auerbach, MS**[1,4], **Qiuming Gong, MD, PhD**[3], **Zhengfeng Zhou, MD, PhD**[3], **Omer Berenfeld, PhD**[1], and **José Jalife, MD**[1,2]

[1]Center for Arrhythmia Research, University of Michigan, Ann Arbor, MI 48108, USA

[2]Department of Molecular and Integrative Physiology, University of Michigan, Ann Arbor, MI 48108, USA

[3]Division of Cardiovascular Medicine, Oregon Health and Science University, Portland, OR 97239, USA

[4]Department of Pharmacology, SUNY Upstate Medical University, Syracuse, NY 13210, USA

Abstract

Rationale—The rapid delayed rectifier potassium current, I_{Kr}, which flows through the human ether-a-go-go-related (hERG) channel is a major determinant of the shape and duration of the human cardiac action potential (APD). However, it is unknown whether the time dependency of I_{Kr} enables it to control APD, conduction velocity (CV) and wavelength (WL) at the exceedingly high activation frequencies that are relevant to cardiac reentry and fibrillation.

Objective—To test the hypothesis that upregulation of hERG increases functional reentry frequency and contributes to its stability.

Methods and Results—Using optical mapping, we investigated the effects of I_{Kr} upregulation on reentry frequency, APD, CV and WL in neonatal rat ventricular myocyte (NRVM) monolayers infected with GFP (control), hERG (I_{Kr}), or dominant negative mutant hERG G628S. Reentry frequency was higher in the I_{Kr}-infected monolayers (21.12±0.8 Hz; n=43 vs. 9.21±0.58 Hz; n=16; p<0.001), but slightly reduced in G628S-infected monolayers. APD_{80} in the I_{Kr}-infected monolayers was shorter (>50%) than control during pacing at 1 to 5 Hz. CV was similar in both groups at low frequency pacing. In contrast, during high frequency reentry, the CV measured at varying distances from the center of rotation was significantly faster in I_{Kr}-infected monolayers than controls. Simulations using a modified NRVM model predicted that rotor acceleration was due in part to a transient hyperpolarization immediately following the AP. The transient hyperpolarization was confirmed experimentally.

Address for correspondence José Jalife, M.D., Center for Arrhythmia Research, University of Michigan, 5025 Venture Drive, Ann Arbor, MI 48108, Phone: 734-998-7578, Fax: 734-998-7711 jjalife@umich.edu.
Luqia Hou and Makarand Deo contributed equally to this study

Subject codes: 132, 152

Disclosures: None.

Conclusion—hERG overexpression dramatically accelerates reentry frequency in NRVM monolayers. Both APD and WL shortening, together with transient hyperpolarization, underlies the increased rotor frequency and stability.

Keywords

hERG; delayed rectifier potassium channel; reentry; ventricular fibrillation; optical mapping

Introduction

Ventricular fibrillation (VF) is a major cause of sudden cardiac death. Evidence suggests that, in mammalian species ranging in size from the mouse to human, VF may be maintained by highly periodic reentrant waves called rotors.[1, 2] The spiral waves that emanate from high frequency rotors propagate through the ventricles, and undergo intermittent, spatially distributed wavebreaks resulting in complex patterns of conduction also known as fibrillatory conduction.[1, 3] While the existence of rotors has been known for years, the ionic mechanisms responsible for their behavior remain incompletely understood. Recently, it was shown that the frequency and the stability of rotors are determined in great measure by the resting membrane potential (RMP) and the conduction velocity (CV), which are controlled by the dynamic interplay between the outward component of the inward rectifier potassium current (I_{K1}) and the rapid inward sodium current (I_{Na}).[4] Other experiments have demonstrated that overexpression of the slow delayed rectifier current (I_{Ks}) does not affect reentry frequency, but significantly increases the incidence of fibrillatory conduction in cardiomyocyte monolayers.[5] However, the consequences of upregulation or gain of function in the rapid delayed rectifier current (I_{Kr}) on reentry frequency and dynamics has never been directly investigated either in the heart or any model system.

The human ether-a-go-go-related (hERG) potassium channel responsible for I_{Kr} is important in determining the shape and duration of the human cardiac action potential (AP).[6] I_{Kr} suppression results in action potential duration (APD) prolongation, cardiac arrhythmias and sudden cardiac death.[7] hERG mutations are associated with chromosome 7-linked inherited long QT syndrome type 2 (LQTS2).[8] In addition, drug induced LQTS is often the result of I_{Kr} blockade.[7] However, an arrhythmogenic phenotype is not limited to loss of function in I_{Kr}.

Recently, a gain-of-function mutation in hERG, N588K, was identified to be associated with short QT syndrome (SQTS).[9] It provided evidence that upregulation of I_{Kr} could be arrhythmogenic. Thus, it seems reasonable to speculate that once a reentrant arrhythmia is initiated, I_{Kr} upregulation influences its dynamics. However, while I_{Kr} contributes significantly to APD, and thus ventricular refractoriness and wavelength (WL ≈ APD×CV) at physiological heart rates, it is unknown whether its time dependency enables it to control the same parameters at the exceedingly high activation rates of cardiac reentry and fibrillation. Therefore the objective of this study was to systematically determine how expression levels of I_{Kr} affect the frequency, stability, and duration of rotors in 2-dimensional neonatal rat ventricular myocyte (NRVM) monolayers. We tested the hypothesis that through its direct effects of APD shortening, upregulation of hERG increases functional reentry frequency and contributes to its stability.

Materials and Methods

Isolation and Culture of NRVM Monolayers

The isolation and culture techniques are described elsewhere.[5] Briefly, hearts from 1 to 2 day old neonatal Sprague-Dawley rats (Charles River, Mass) were removed and collected in

calcium and magnesium free Hanks' Balanced Salt Solution (HBSS). Then the ventricles were isolated, minced and enzymatically digested in a solution that contained 0.06% trypsin (Roche Applied Science) and 0.15% pancreatin (Sigma). After a two-hour preplating period, which helped avoid non-cardiomyocyte attachment, cells were cultured in M199 medium (Cambrex) with 10% fetal bovine serum (FBS) (Cellgro), 20 U/mL penicillin, 20 μg/mL streptomycin, and 100 μmol/L bromodeoxyuridine (Sigma). Finally, myocytes were plated in 35 mm tissue culture dishes at a density of $1x10^6$ cells/dish for monolayers and at low density on 25 mm cover slips for single cell patch-clamp experiments. To facilitate cardiomyocyte attachment, dishes were coated with human placental collagen type IV (Sigma). Cells were subsequently cultured at 37°C, 5% CO_2.

Adenoviral Construct

We generated adenoviral constructs containing WT or G628S cDNA sequence of hERG tagged with GFP, using the AdEasy vector system (Stratagene, La Jolla, CA) as described in 10 and in the online supplement (OLS).

Electrophysiology

In whole-cell patch-clamp experiments the bath solution was HBSS with Ca^{2+} and Mg^{2+} (Sigma); pH was adjusted to 7.4 with NaOH. Nifedipine (5 μM) and 4-AP (2 mM) were added to reduce extraneous ion currents. The pipette solution contained (in mM): 1 $MgCl_2$, 5 EGTA, 150 KCl, 5 HEPES, 5 Phosphocreatine, 4.5 K_2ATP, 2mM B-hydroxybutyric acid; pH was adjusted to 7.2 with KOH. Recordings were carried out at 37°C using a MultiClamp 700B amplifier (Axon Instruments, Forest City, CA). After gigaseal formation and patch break the tip potential was nulled and cell capacitive currents and series resistance were optimally (~80%) compensated. I_{Kr} currents were elicited with 0.5-second depolarizing steps applied in 10 mV increments from a holding potential of −60 mV to +50 mV. I_{Kr} was derived by subtracting currents recorded in the presence of E4031 (1 μM) from control currents.

APs were recorded from individual myocytes using the current-clamp mode of the MultiClamp 700B amplifier after gigaseal formation and patch break. Stimulus pulses (1–2 ms duration) were generated using a World Precision Instruments DS8000 stimulator. The bath solution was HBSS with Ca^{2+} and Mg^{2+} (Sigma). The pipette solution contained (in mM): 1 $MgCl_2$, 5 EGTA, 150 KCl, 5 HEPES, 5 Phosphocreatine, 4.5 K_2ATP, 2mM B-Hydroxybutyric acid. Recordings were carried out at 37 °C.

Optical mapping

High-resolution optical mapping was conducted using a CCD camera (80x80 pixels, SciMeasure). Cultured dishes were placed on a heating chamber connected and maintained at 37°C. Monolayers were superfused with HBSS (in mM/L): 1.6 $CaCl_2$, 5.4 KCl, 0.8 $MgSO_4$, 0.4 KH_2PO_4, 4.2 $NaHCO_3$, 136.9 NaCl, 0.3 $NaHPO_4$, 5.5 D-Glucose, and 10 HEPES; pH 7.4. Electrical wave propagation was recorded by staining the cells with 40 μM/L di-8-ANEPPS (Molecular Probes) for 15 minutes. We obtained 5-seconds movies at 200 frames/s and 2-seconds movies at 500 frames/s.

Data Analysis

Please refer to the OLS for pacing protocols, patch clamp data analysis and optical mapping data processing and analysis.

Computer Simulations—We have modified an existing mathematical model of the neonatal rat myocyte published by Korhonen et al.13 This model is unique in that the

cytosolic Ca^{2+} is a function of temporal as well as spatial coordinates. Due to the lack of t-tubules,14 calcium ions entering into the cells via membrane channels must diffuse a small distance through the cytosol before reaching the sarcoplasmic reticulum and trigger the excitation-contraction coupling machinery. Some ionic current components were modified to reproduce the AP morphology and the restitution properties recorded from the experiments performed in our laboratory. (Details in the Online Supplement)

Statistical Analysis—Data are expressed as mean±SEM. Patch-clamp data were analyzed by two-way ANOVA with Bonferroni post-tests. Analyses of reentry frequency were performed using one-way ANOVA with Tukey's multiple comparison test. A Student's *t test* with Welch-correction was used to analyze the average APD and CV, as well as the maximal diastolic potential (MDP) data. $p<0.05$ was considered to be significant.

Results

hERG overexpression upregulates I_{Kr} in NRVM

At 200 or 30 MOI of adenoviral expression, we observed maximal GFP-tagged WT or G628S mutant hERG channel expression in NRVM monolayers. Spatially uniform protein expression was consistently confirmed by fluorescent microscopy as illustrated in Figure 1A.

Figure 1B illustrates on the top the voltage-clamp protocol (see Methods) used to determine the voltage dependence of I_{Kr} density. The same panel shows superimposed representative I_{Kr} traces recorded from single NRVM infected with Ad-GFP (middle) or Ad-hERG (bottom). The K^+-carried I_{Kr} current was appreciably increased in the Ad-hERG infected myocytes when compared to control. As summarized in Figure 1C, Ad-hERG infected cells have a significantly steeper current density vs voltage (IV) relation than Ad-GFP control. At 0 mV, outward current was 14.7 ± 1.98 pA/pF in cells expressing hERG versus 2.8 ± 0.53 pA/pF in cells expressing GFP ($p<0.001$). As shown in panel D, the peak tail current also increased significantly in Ad-hERG myocytes. However, activation of the normalized tail current showed no kinetic difference between the two groups (Figure 1E).

I_{Kr} upregulation accelerates reentry frequency

Sustained functional reentry could be obtained from monolayers infected by Ad-GFP, Ad-hERG and Ad-G628S. Figure 2A shows phase maps of single rotors generating spiral waves in Ad-GFP control (left), I_{Kr}-overexpressing (middle), and G628S-overexpressing (right) monolayers. The corresponding color activation maps and time space plots demonstrating the stability and reproducibility of the respective reentry patterns are presented in Online Figures I and II. The graph in Figure 2B compares the ranges of individual rotation frequencies of control monolayers with that of I_{Kr}-overexpressing and G628S-overexpressing monolayers. The mean values are shown as horizontal bars for each experimental group. The average frequency is significantly higher in I_{Kr}-overexpressing monolayers than GFP controls (21.12±0.81, n = 43; vs. 9.21±0.58 Hz, n = 16; $p<0.001$); whereas the frequency in the G628S monolayers is slightly lower (6.14±0.3 Hz, n=17; NS vs GFP).

To confirm the involvement of I_{Kr} overexpression on the acceleration of rotor frequency, E4031, a specific I_{Kr} blocker, was superfused at a concentration of 1μM in 23 monolayers infected with Ad-hERG. As shown in Figure 3, E4031 dramatically reduced the frequency of rotation (22.75±1.24 vs. 9.82±0.74 Hz, $p<0.05$). This effect was partially reversed after a 5min washout period (16.72±1.03 Hz, $p<0.05$ vs. E4031).

Wavelength shortening underlies I_{Kr}-induced rotor acceleration

To elucidate the mechanism by which hERG accelerated reentry frequency, we first investigated the effect of I_{Kr} overexpression on APD and CV during pacing at varying cycle lengths. From high-resolution APD maps, APD_{80} was measured during 1:1 activation in 11 control and 8 I_{Kr} overexpressing monolayers. Online Figure III shows examples of single pixel recordings at pacing cycle lengths between 1000 and 200 ms. The data demonstrates the excellent signal-to-noise ratio, which allowed accurate APD measurements. As shown in Figure 4A, I_{Kr} expression reduced the APD_{80} by more than 50% when compared with control during pacing at cycle length between 200 and 1000ms ($p<0.01$). On the other hand, as shown in Figure 4B, the mean CV of Ad-hERG expressing monolayers was similar to Ad-GFP monolayers at all pacing cycle lengths. Moreover, the wavelength (WL = APDxCV), was significantly shorter in the Ad-hERG monolayers than the control group at all pacing cycle length (Figure 4C).

We also plotted the rotation frequency in each monolayer as a function of the respective mean APD_{80} in both control and I_{Kr} overexpressing groups. As shown in Figure 5A, the relationship was very steep and highly significant for the Ad-hERG group. In some monolayers, hERG overexpression reduced APD_{80} less than 30 ms, which enabled rotation frequencies of 25 Hz or higher. In contrast in the Ad-GFP group, although the slope of the relationship was significant, it was much less steep and the minimal APD_{80} was 60ms and the highest rotation frequency was 12.6 Hz.

As demonstrated previously,[4, 15, 16] during functional reentry, the CV decreases as the curvature of the wavefront increases toward the center of rotation (core). We therefore measured the CV as a function of distance from the core to determine whether I_{Kr} affected that relationship in the same manner as I_{K1} overexpression does.[4] In Figure 5B we summarize data for 21 Ad-hERG monolayers and 12 Ad-GFP monolayers. As expected, CV increased gradually as a function of distance from the core in both groups. However, the Ad-hERG monolayers showed a lager CV at all distances from the core as compared with the Ad-GFP monolayers ($p<0.05$). Similarly, the curvature of the wavefront near its pivot point was determined and compared between groups (see Online Figure IV for details). Curvature was larger in the Ad-hERG monolayers than Ad-GFP controls. Taken together, this analysis showed that during reentry, excitability and CV are higher in the Ad-hERG monolayers than in the Ad-GFP control.

Figure 5C shows a comparison of WL measured during reentry as the expanse between the wavefront and the end of the repolarization wavetail (for details see Online Figure XI and corresponding text in the Online Supplement). As expected, the WLs were significantly shorter in the Ad-hERG group. They ranged between 2.75 and 6.89 mm, whereas control WLs ranged between 7.88 and 22.22 mm ($p<0.05$). Altogether the data presented thus far suggested that APD and WL shortening, together with increased CV underlie rotor acceleration in I_{Kr}-upregulated monolayers.

Numerical Simulations

To gain further mechanistic insight into the effects of hERG overexpression on rotor frequency and stability, we conducted computer simulations at the single cell level, as well as in 2D using a modified model of the NRVM (for details see Online Figures V-IX and corresponding text in the Online Supplement). Figure 6A shows APs elicited in the single cell model by pacing at 1 Hz in control, and hERG increase (I_{Kr} 5.21X). As expected, APD abbreviated upon I_{Kr} upregulation. Interestingly, in the I_{Kr} 5.21X model the AP was followed by a highly reproducible transient hyperpolarization (see also Figure 7A).

We investigated the consequences of I_{Kr} upregulation on rotor dynamics in a 2D monolayer model. As shown in Figure 6B, the reentry frequency was significantly increased from 12.8 Hz in control to 18.5 Hz in I_{Kr} 5.21X, which was consistent with the experimental result shown in Figure 2. Similar to experiments, overexpressing I_{Kr} (5.21X) in the simulations increased the CV during reentry at all distances from the core compared with the controls (Figure 6C).

To determine whether the changes seen in Figure 6A had any role in I_{Kr} overexpression-induced rotor acceleration, we subjected the single cell model to pacing at varying frequencies (from 1 to 20 Hz). We surmised that at the highest frequencies the ensuing APD shortening and transient hyperpolarization should increase I_{Na} availability and therefore excitability. To test that hypothesis, the fast inward sodium current (I_{Na}) was recorded in two sets of simulations (control, and I_{Kr} 5.21X, respectively), and peak I_{Na} was plotted against pacing frequency for each case. As a negative control, in yet another set of simulations we scaled I_{Ks} (25X) while I_{Kr} was kept unchanged. Differences in cell excitability were investigated in both sets in terms of peak I_{Na} amplitude. As shown in Figure 7A, while I_{Kr} upregulation produced a concomitant transient hyperpolarization after the abbreviated action potential (left), I_{Ks} upregulation did not result in membrane hyperpolarization (top right). Therefore, as shown in Figure 7B, the effects of I_{Ks} upregulation on I_{Na} availability were substantially less at any given activation frequency, compared with the effects of I_{Kr} upregulation. The difference was most significant at the highest frequencies between 12 and 20 Hz. This could explain the effect of I_{Kr} upregulation on CV increase during high frequency reentry (Figure 5B) but not low frequency pacing (Figure 4B).

As discussed above in Figure 5A, the slope of the line defining the relationship between rotation frequency and APD was steeper in the case of hERG overexpression than in control. We surmised that such an increase in the sensitivity of rotation frequency to APD abbreviation was the result of the transient hyperpolarization. Therefore, we studied the effects of premature stimuli (S1-S2 protocol) in single cell, 1D cable and 2D monolayer models (see Online Figure X). In Panel C of Figure 7, a single I_{Kr} 5.21X cell was paced at 2 Hz (S1) for 10 seconds followed by a premature stimulus (S2) at varying intervals. It is clear from that graph that at the shorter S2 intervals, more I_{Na} was activated in I_{Kr} 5.21X model compared to control. This increase in peak I_{Na} disappeared when the transient membrane hyperpolarization was suppressed by clamping the maximal diastolic potential (MDP) to −70 mV. As illustrated in panel A of figure S10, in the 1D cable of 10 mm in length, this increase in I_{Na} translated into increased CV which again disappeared when the MDP was clamped to −70 mV. We further verified the role of the transient hyperpolarization during reentry in 2D monolayer models by clamping the MDP to various voltages. As expected, the frequency of reentry was progressively reduced with increasing the value of MDP (see panel B of Online Figure X. The clamped voltages in these simulations covered the range of our experimentally observed MDPs and thus clearly underscored the role of the transient hyperpolarization in addition to the APD abbreviation in increasing the rotor frequency and CV during reentry in I_{Kr} upregulation.

I_{Kr}-Induced transient hyperpolarization in NRVM

To determine whether a transient hyperpolarization predicted by simulations occurred experimentally in the in NRVM, we obtained single cell action potential recordings using current clamp. In Figure 8A, we present 2 representative action potential recordings at a pacing cycle length of 2000 ms. Consistent with the simulation results, APD shortening and a transient hyperpolarization were demonstrated in the myocytes infected with Ad-hERG when compared to Ad-GFP. In Figure 8B, we quantified the MDP after each action potential in Ad-hERG (−67.6±0.98 mV; n= 8) and Ad-GFP cells (−63.9±1.11 mV; n=6; p=0.03). As

shown in Figure 8C, APD was measured at three different levels (APD_{30}, APD_{50} and APD_{80}) and showed a significant reduction when hERG was overexpressed. Taken together, these results demonstrated that APD shortening and transient hyperpolarization are both important consequences of I_{Kr} overexpression.

Discussion

We have investigated the consequences of I_{Kr} upregulation on electrical impulse propagation and reentry dynamics in 2-D biological and numerical models. The most important results are as follows: 1. I_{Kr} overexpression significantly increased the frequency of reentry. 2. During pacing at 1-5Hz, I_{Kr} overexpression shortened APD and WL more than 50%, but did not affect the CV. 3. During sustained reentry, rotation frequency demonstrated a steep and highly significant dependence on I_{Kr} upregulation-induced shortening of APD. The CV was significantly larger in the hERG group vs. the control group at all distances from the core. In addition, the WL was significantly shorter in Ad-hERG monolayers than in control. 4. Computer simulations and single cell action potential recordings demonstrated that APD shortening and the transient hyperpolarization after each AP in hERG overexpressing NRVM increased the INa availability, which contribute to the increased rotor frequency.

Pathophysiological implications

The contribution of I_{Kr} to repolarization has been recognized for decades.17 Since hERG was identified from a human hippocampal cDNA library in 1994,18 more than 300 mutations have been found to be associated with LQTS2.8 These mutations result in suppression of hERG channel function, either by impaired trafficking or dominant negative effect of channel subunits on channel function.8 Gain-of-function mutations have been found as well. Recently, a hERG-linked short-QT syndrome was identified with an inactivation-attenuating hERG channel mutation.9, 19, 20

A dual mechanism for I_{Kr}-overexpression-induced rotor acceleration

While the clinical phenotypes associated with alterations in potassium channels have been characterized for years, it was unknown how those alterations affected reentry frequency and dynamics. The results of our study suggest that the consequences of I_{Kr} overexpression are somewhat similar to those recently demonstrated for the ventricles of transgenic mice overexpressing the inward rectifier potassium channel (I_{K1}), which resulted in a shorter WL, sustained membrane hyperpolarization and exceedingly fast and stable reentry/VF.4 In the same study, computer simulations established that during sustained reentry the diastolic membrane potential was 4 mV more negative (~−94 mV) in the transgenic when compared to the WT case (~−90 mV). Such hyperpolarization was enough to increase the Na^+ channel availability by ~30%, which contributed to reducing the core size and stabilizing the reentry. Similar to the I_{K1} overexpressing mouse, our I_{Kr} overexpressing monolayers also resulted in APD and WL shortening. However, unlike the transgenic I_{K1} overexpressing mouse, the hyperpolarization associated with I_{Kr} overexpression was transient and the membrane potential returned to the resting level within 100 msec or less (Figures 6 and 8). Therefore, a relative increase in CV was manifest during high frequency reentry, but was undetectable at the lower pacing frequencies.

Nevertheless, as demonstrated by additional computer simulations presented in Figure 7, increase in Na^+ channel availability at the time of maximal hyperpolarization would certainly contribute to increase the CV (also see Figure S10), hence the frequency and stability of the rotors and to reduce the incidence of wavebreak and fibrillatory conduction. Initially, this was quite unexpected because upregulation of the other component of the

delayed rectifier K^+ current, I_{Ks}, has been shown to contribute to post-repolarization refractoriness, and to increase the incidence of wavebreaks and fibrillatory conduction, with only a modest increase in rotor frequency.5 Yet as demonstrated in the computer simulation (Figure 7), while I_{Kr} upregulation produced a transient hyperpolarization after the abbreviated action potential, I_{Ks} upregulation did not result in membrane hyperpolarization and therefore its effects on I_{Na} availability were substantially blunted at any given activation frequency. The difference is most significant at the highest frequencies which are relevant to those usually observed during reentry in the monolayers. Our additional computer simulations presented in online Figure X with MDPs clamped to less negative potentials in single cell, 1D cable and 2D monolayer models further confirm that the transient hyperpolarization contributes to the acceleration of reentry in I_{Kr} upregulation. Note that the effects of increased I_{Na} availability and CV disappeared when the transient hyperpolarization was artificially suppressed.

Different I_{Kr} vs I_{Ks} kinetics, different consequences during reentry

Although counterintuitive, the above results add up when one considers the different kinetics of I_{Kr} and I_{Ks}, as well as their different contributions to repolarization. I_{Kr} activates rapidly and displays marked inward rectification due to the fact that, at positive membrane potentials, the rate of I_{Kr} inactivation is faster than the rate of I_{Kr} activation.21 Consequently, I_{Kr} has a relatively low conductance during the AP plateau (phase 2) but continues to increase throughout a substantial portion of the repolarization phase (Figure 7A), which explains the marked APD shortening and transient hyperpolarizing effects of I_{Kr} overexpression in our NRVMs. In contrast, although I_{Ks} increases somewhat more rapidly during the plateau, it already begins to decline before phase-3 repolarization takes place (Figure 7B). As such I_{Ks} contributes relatively less than I_{Kr} to the repolarization of the ventricular APs and thus its APD shortening effect is relatively less than I_{Kr} at any given level of upregulation (data not shown). This, together with the fact that I_{Ks} upregulation does not lead to transient hyperpolarization after each action potential, helps explain the substantially lesser effect of I_{Ks} upregulation on rotor frequency in the monolayers than I_{Kr} upregulation. In addition, as demonstrated previously,4,22,23 because of its slow deactivation kinetics I_{Ks} will tend to accumulate at high frequencies and therefore play an important role in postrepolarization refractoriness,22,23 and fibrillatory conduction.4 In contrast, during reentry the shorter APD produced by I_{Kr}-overexpression gives Na^+ channels enough time to recover, without impinging on the excitability during the diastolic interval before the next wavefront invades the tissue, thus avoiding wavefront-wavetail interactions that could destabilize the rotor. In addition, the transient hyperpolarization induced by I_{Kr} upregulation further increases Na^+ channel availability and excitability, both of which are very sensitive to the membrane potential. Finally, I_{Kr} is not known to accumulate, which would make it unlikely to play any important role in postrepolarization refractoriness, and would explain why, in the I_{Kr}-overexpressing monolayers, the spiral waves are able to rotate at very high frequencies without breaking.

Study Limitations

The effect of hERG was examined in the NRVM monolayer model, which allowed us to overexpress hERG channel and study its effect on reentry dynamics in a highly controlled environment. However, by overexpressing the hERG channel alone we have not considered the importance that the regulatory β-subunits have in reconstituting native I_{Kr},24 or their role in controlling reentry frequency. Further, the consequences of channel expression in neonatal rodent myocytes are likely to be different from those in human adult myocytes since the ionic profile is different. Also, the closeness of the RMP to the K^+ equilibrium potential in normally polarized adult cardiomyocytes would substantially diminish the contribution of the transient hyperpolarization to the overall effect observed in NRVMs.

However, reentry typically occurs in association with ischemia/reperfusion injury—a situation in which external K^+ is usually elevated—therefore, depolarization of the RMP may increase the relevance of the latter mechanism in the adult heart. Finally, the conclusions that have been drawn from this study are only conceptual and mechanistic in relation to the cardiac fibrillatory process. In no way do we attempt to relate them to the clinical setting. Further studies in translational models would be necessary before any extrapolation to humans can be made.

Conclusion

This is the first study to systematically evaluate the role of I_{Kr} in the frequency and stability of reentry. We demonstrate that hERG overexpression dramatically accelerates reentry frequency in NRVM monolayers. APD shortening and transient hyperpolarization induced increase in excitability are the mechanisms underlying reentry acceleration.

Novelty and Significance

What Is Known?

- The human ether-a-go-go-related (hERG) potassium channel responsible for the rapid component (I_{Kr}) of the delayed rectifier current IK is important in determining the shape and duration of the human cardiac action potential.
- Alterations in the density of I_{Kr} change the action potential duration (APD) and may result in cardiac arrhythmias and sudden cardiac death.
- Gain-of-function mutation in hERG (N588K) leads to short QT syndrome, indicating that an increase in I_{Kr} could be arrhythmogenic.

What New Information Does This Article Contribute?

- Overexpression of IKr significantly alters the frequency and stability of functional reentry; the mechanism underlying ventricular tachyarrhythmias including fibrillation, the most dangerous type of cardiac arrhythmia.
- The increase in reentry frequency depends on APD abbreviation and wavelength shortening, as well as on transient hyperpolarization of the resting membrane potential.
- Transient hyperpolarization increases the sodium channel availability and cellular excitability and therefore contributes significantly to an increase in reentry frequency.

Summary

Both loss- and gain-of-function mutations in hERG have been associated with cardiac arrhythmias and sudden death. The data presented in this paper demonstrate, for the first time, a direct link between I_{Kr} density and reentry dynamics. The increase in frequency of reentry was achieved not only by a shortening of APD and wavelength, but also by transient hyperpolarization of phase 4 of the action potential. These findings extend our understanding of the molecular mechanisms of ventricular fibrillation and complement previous studies which strongly suggest that repolarizing potassium currents contribute to fibrillation.

Supplementary Material

Refer to Web version on PubMed Central for supplementary material.

Non-standard Abbreviations and Acronyms

hERG	human ether-a-go-go-related gene
AP	action potential
APD	action potential duration
CV	conduction velocity
WL	wavelength
RMP	resting membrane potential
MDP	maximum diastolic potential
NRVM	neonatal rat ventricular myocyte
LQTS	long QT syndrome
SQTS	short QT syndrome
VF	ventricular fibrillation
I_{Kr}	cardiac rapid delayed rectifier current
I_{Ks}	cardiac slow delayed rectifier current
I_{K1}	inward rectifier current
NS	not significant

Acknowledgments

Sources of Funding

Supported by NHLBI Grants P01-HL039707, P01-HL087226; R01-HL080159 and R01 HL60843 (JJ), and R01-HL68854 (ZZ).

References

1. Jalife J. Ventricular fibrillation: mechanisms of initiation and maintenance. Annu Rev Physiol. 2000; 62:25–50. [PubMed: 10845083]
2. Noujaim SF, Berenfeld O, Kalifa J, Cerrone M, Nanthakumar K, Atienza F, Moreno J, Mironov S, Jalife J. Universal scaling law of electrical turbulence in the mammalian heart. Proc Natl Acad Sci U S A. 2007; 104:20985–20989. [PubMed: 18093948]
3. Jalife, J.; Delmar, M.; Anumonwo, J.; Berenfeld, O.; Kalifa, J., editors. Basic Cardiac Electrophysiology for the Clinician. A John Wiley & Sons, Ltd.; 2009. Publication
4. Noujaim SF, Pandit SV, Berenfeld O, Vikstrom K, Cerrone M, Mironov S, Zugermayr M, Lopatin AN, Jalife J. Up-regulation of the inward rectifier K+ current (I K1) in the mouse heart accelerates and stabilizes rotors. J Physiol. 2007; 578:315–326. [PubMed: 17095564]
5. Munoz V, Grzeda KR, Desplantez T, Pandit SV, Mironov S, Taffet SM, Rohr S, Kleber AG, Jalife J. Adenoviral expression of IKs contributes to wavebreak and fibrillatory conduction in neonatal rat ventricular cardiomyocyte monolayers. Circ Res. 2007; 101:475–483. [PubMed: 17626898]
6. Sanguinetti MC, Tristani-Firouzi M. hERG potassium channels and cardiac arrhythmia. Nature. 2006; 440:463–469. [PubMed: 16554806]
7. Hancox JC, McPate MJ, El Harchi A, Zhang YH. The hERG potassium channel and hERG screening for drug-induced torsades de pointes. Pharmacol Ther. 2008; 119:118–132. [PubMed: 18616963]
8. Perrin MJ, Subbiah RN, Vandenberg JI, Hill AP. Human ether-a-go-go related gene (hERG) K+ channels: function and dysfunction. Prog Biophys Mol Biol. 2008; 98:137–148. [PubMed: 19027781]

9. Brugada R, Hong K, Dumaine R, Cordeiro J, Gaita F, Borggrefe M, Menendez TM, Brugada J, Pollevick GD, Wolpert C, Burashnikov E, Matsuo K, Wu YS, Guerchicoff A, Bianchi F, Giustetto C, Schimpf R, Brugada P, Antzelevitch C. Sudden death associated with short-QT syndrome linked to mutations in HERG. Circulation. 2004; 109:30–35. [PubMed: 14676148]
10. Gong Q, Zhang L, Vincent GM, Horne BD, Zhou Z. Nonsense mutations in hERG cause a decrease in mutant mRNA transcripts by nonsense-mediated mRNA decay in human long QT syndrome. Circulation. 2007; 116:17–24. [PubMed: 17576861]
11. Berenfeld O, Zaitsev AV, Mironov SF, Pertsov AM, Jalife J. Frequency-dependent breakdown of wave propagation into fibrillatory conduction across the pectinate muscle network in the isolated sheep right atrium. Circ Res. 2002; 90:1173–1180. [PubMed: 12065320]
12. Mironov S, Jalife J, Tolkacheva EG. Role of conduction velocity restitution and short-term memory in the development of action potential duration alternans in isolated rabbit hearts. Circulation. 2008; 118:17–25. [PubMed: 18559701]
13. Korhonen T, Hanninen SL, Tavi P. Model of excitation-contraction coupling of rat neonatal ventricular myocytes. Biophys J. 2009; 96:1189–1209. [PubMed: 19186154]
14. Delcarpio JB, Claycomb WC, Moses RL. Ultrastructural morphometric analysis of cultured neonatal and adult rat ventricular cardiac muscle cells. Am J Anat. 1989; 186:335–345. [PubMed: 2589218]
15. Tamaddon HS, Vaidya D, Simon AM, Paul DL, Jalife J, Morley GE. High-resolution optical mapping of the right bundle branch in connexin40 knockout mice reveals slow conduction in the specialized conduction system. Circ Res. 2000; 87:929–936. [PubMed: 11073890]
16. Samie FH, Berenfeld O, Anumonwo J, Mironov SF, Udassi S, Beaumont J, Taffet S, Pertsov AM, Jalife J. Rectification of the background potassium current: a determinant of rotor dynamics in ventricular fibrillation. Circ Res. 2001; 89:1216–1223. [PubMed: 11739288]
17. Charpentier F, Merot J, Loussouarn G, Baro I. Delayed rectifier K(+) currents and cardiac repolarization. J Mol Cell Cardiol. 2009
18. Warmke JW, Ganetzky B. A family of potassium channel genes related to eag in Drosophila and mammals. Proc Natl Acad Sci U S A. 1994; 91:3438–3442. [PubMed: 8159766]
19. Gaita F, Giustetto C, Bianchi F, Wolpert C, Schimpf R, Riccardi R, Grossi S, Richiardi E, Borggrefe M. Short QT Syndrome: a familial cause of sudden death. Circulation. 2003; 108:965–970. [PubMed: 12925462]
20. McPate MJ, Duncan RS, Hancox JC, Witchel HJ. Pharmacology of the short QT syndrome N588K-hERG K+ channel mutation: differential impact on selected class I and class III antiarrhythmic drugs. Br J Pharmacol. 2008; 155:957–966. [PubMed: 18724381]
21. Tseng GN. I(Kr): the hERG channel. J Mol Cell Cardiol. 2001; 33:835–849. [PubMed: 11343409]
22. Kurokawa J, Abriel H, Kass RS. Molecular basis of the delayed rectifier current I(ks)in heart. J Mol Cell Cardiol. 2001; 33:873–882. [PubMed: 11343411]
23. Gintant GA. Two components of delayed rectifier current in canine atrium and ventricle. Does IKs play a role in the reverse rate dependence of class III agents? Circ Res. 1996; 78:26–37. [PubMed: 8603502]
24. Abbott GW, Xu X, Roepke TK. Impact of ancillary subunits on ventricular repolarization. J Electrocardiol. 2007 Nov-Dec; 40(6 Suppl):S42–S46. [PubMed: 17993327]

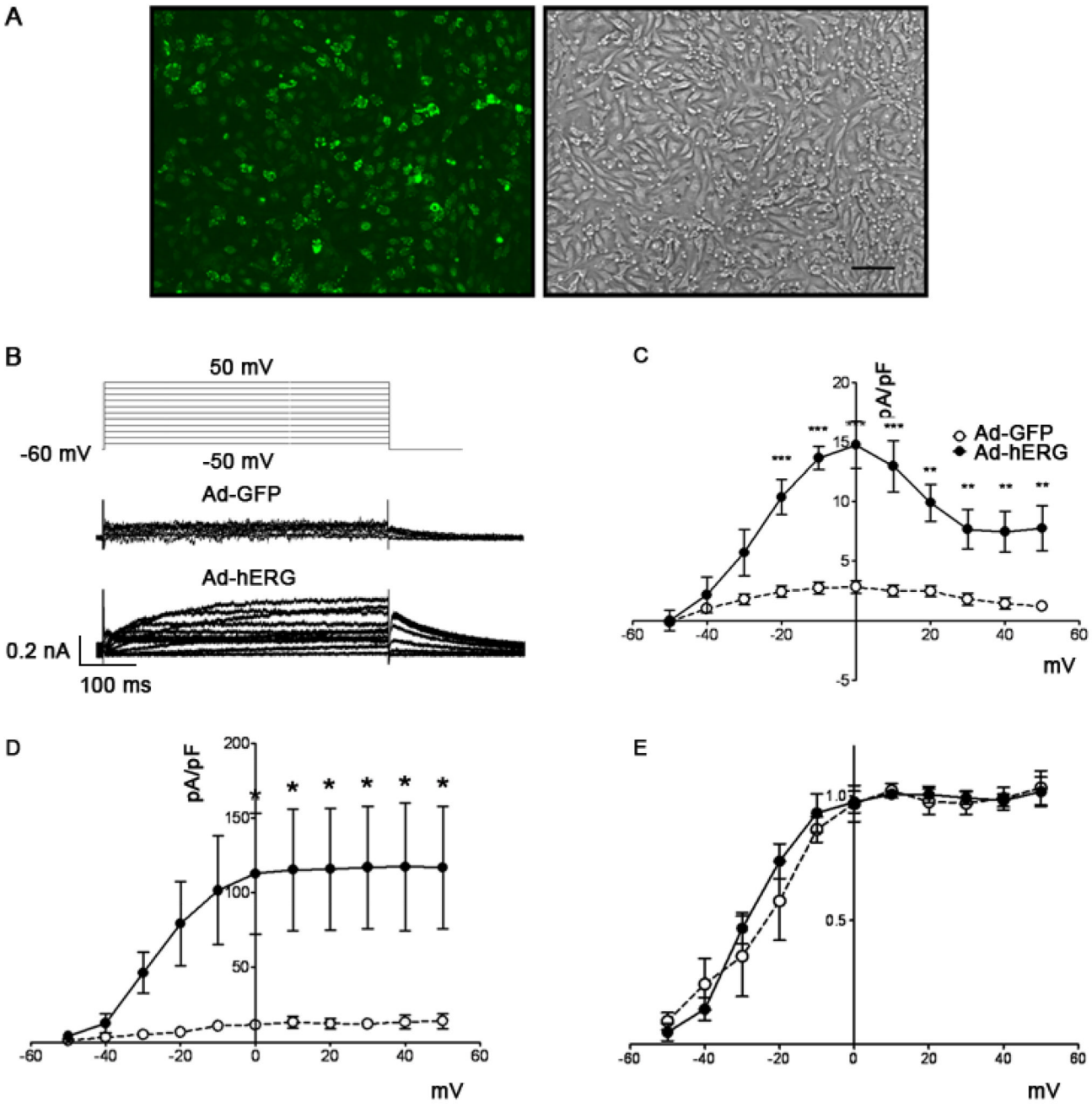

Figure 1.

Adenoviral expression of hERG protein in neonatal rat ventricular cardiomyocytes after 48 hours of infection. **A**. GFP-tagged WT hERG channel expression. Left: fluorescent micrograph of a 4-day-old neonatal rat ventricular myocyte monolayer 48 h after viral infection. Right: corresponding phase contrast micrograph. Scale bar = 100 μm. **B**. Voltage clamp protocol (top) and representative examples of currents from Ad-GFP (middle) and Ad-hERG (bottom) infected myocytes. **C**. I-V relationship of the E4031-sensitive current normalized to cell capacitance in neonatal rat ventricular myocytes infected with Ad-GFP (open circles; n=5) and Ad-hERG (filled circles; n=5). ***$p < 0.001$, **$p < 0.01$, *$p < 0.05$; Ad-hERG vs. Ad-GFP, two-way ANOVA with Bonferroni post-tests. **D**. I-V relationship of

the peak tail currents. **E**. Normalized peak tail currents from Ad-GFP and Ad-hERG myocytes. The two curves are not different statistically.

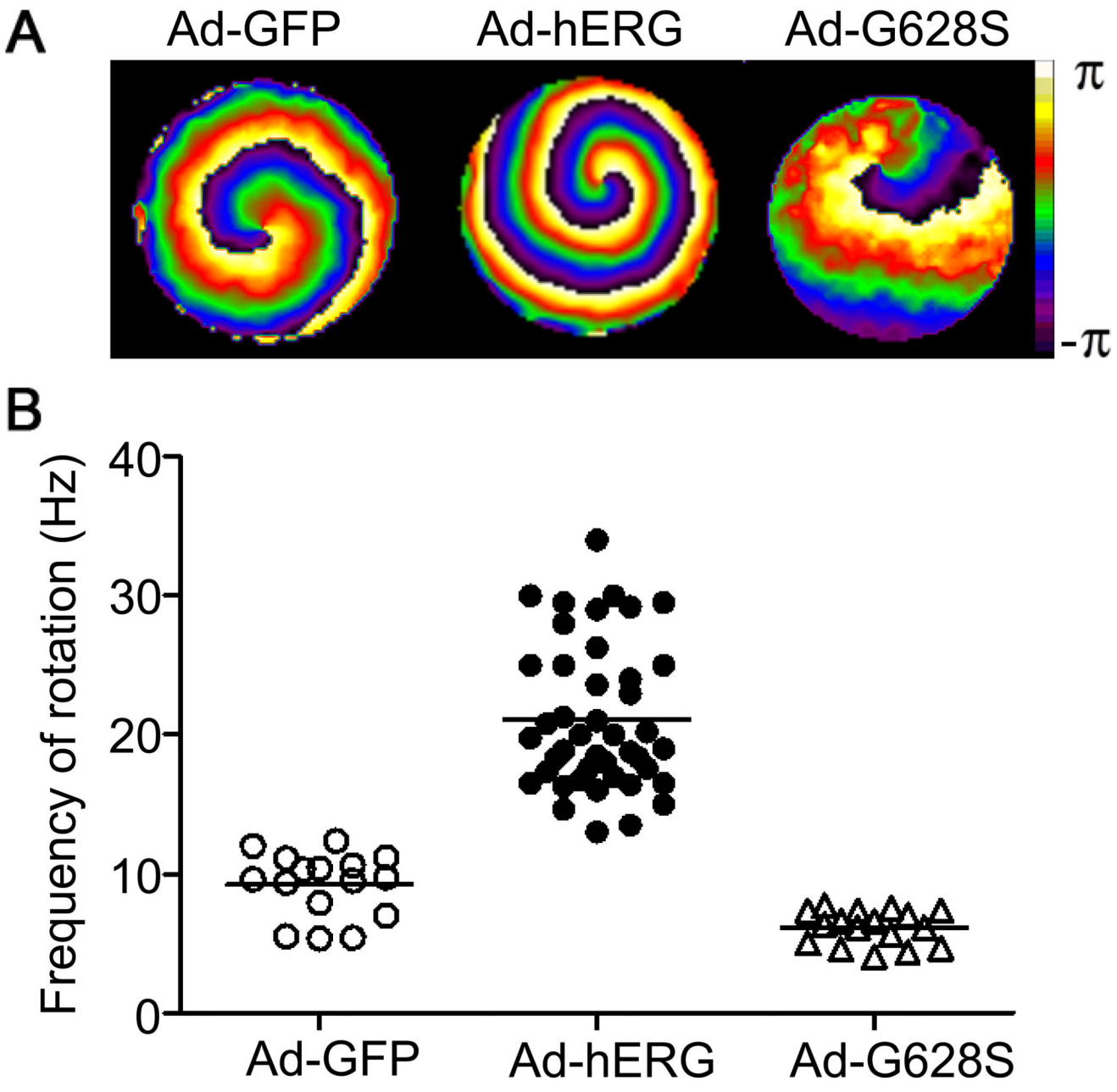

Figure 2.

Effects of hERG infection on reentry frequency in NRVM monolayers. **A**. Snapshots from representative optical mapping movies in monolayers infected with Ad-GFP (left), Ad-hERG (middle), or Ad-G628S (right). **B**. Reentry frequencies in individual monolayers infected with Ad-GFP (open circles), Ad-hERG (closed circles; $p<0.05$ vs. GFP), or Ad-G628S (open triangles; NS vs. Ad-GFP; $p<0.05$ vs. Ad-hERG). Horizontal bars represent mean values. One-way ANOVA with Tukey's multiple comparison test.

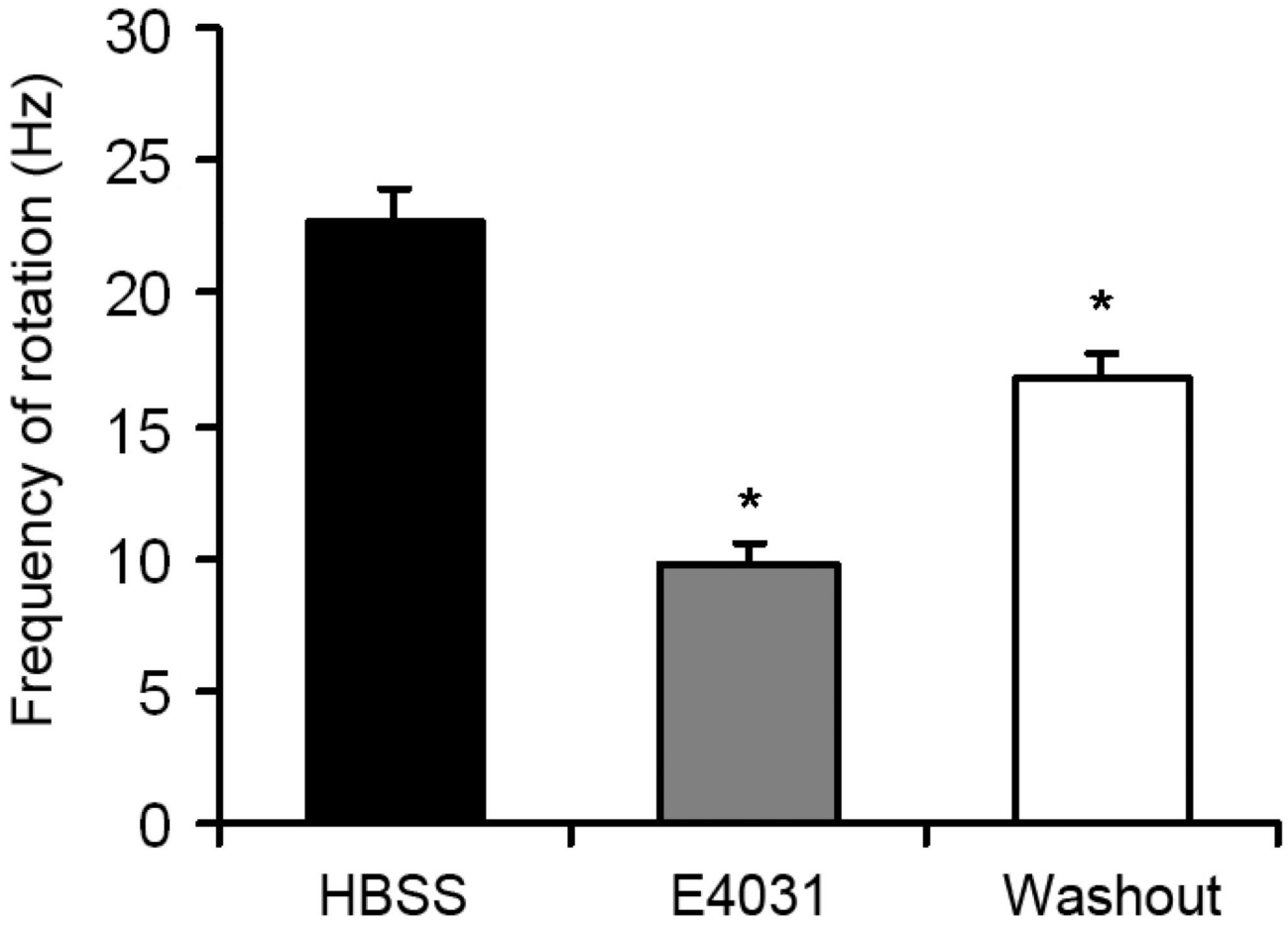

Figure 3.
Effect of E4031 on reentry frequency in I_{Kr} monolayers. Reentry frequencies of hERG overexpressing monolayers before (black) and after (grey) superfusion of E4031; and reentry frequency after 5 min washout (white). One-way ANOVA with Tukey's multiple comparison test.

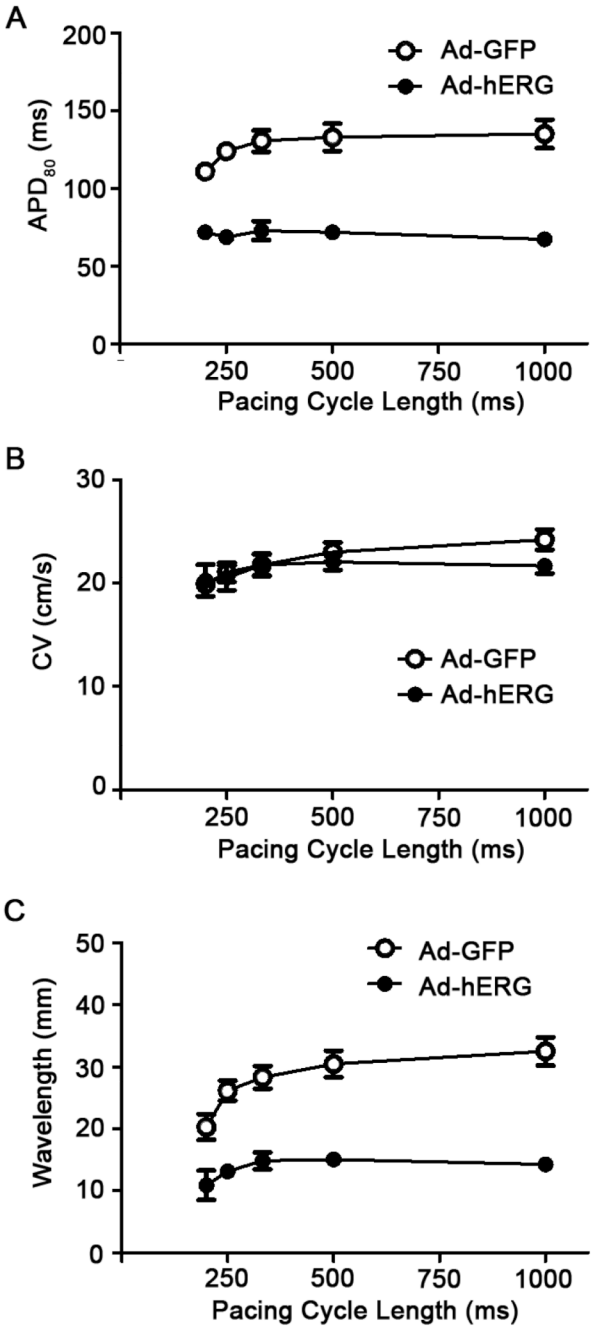

Figure 4.

Effects of hERG overexpression on action potential duration (APD), conduction velocity (CV) and wavelength in monolayers paced at varying frequencies. **A**. Frequency dependence of APD_{80}. Mean values are statistically different ($p<0.05$). **B**. Frequency dependence of CV. Control values are not significantly different (NS) from Ad-hERG values at any pacing frequency; **C**. Frequency dependence of wavelength (WL=CV×APD). Mean values are significantly different at all pacing cycle lengths ($p<0.05$)

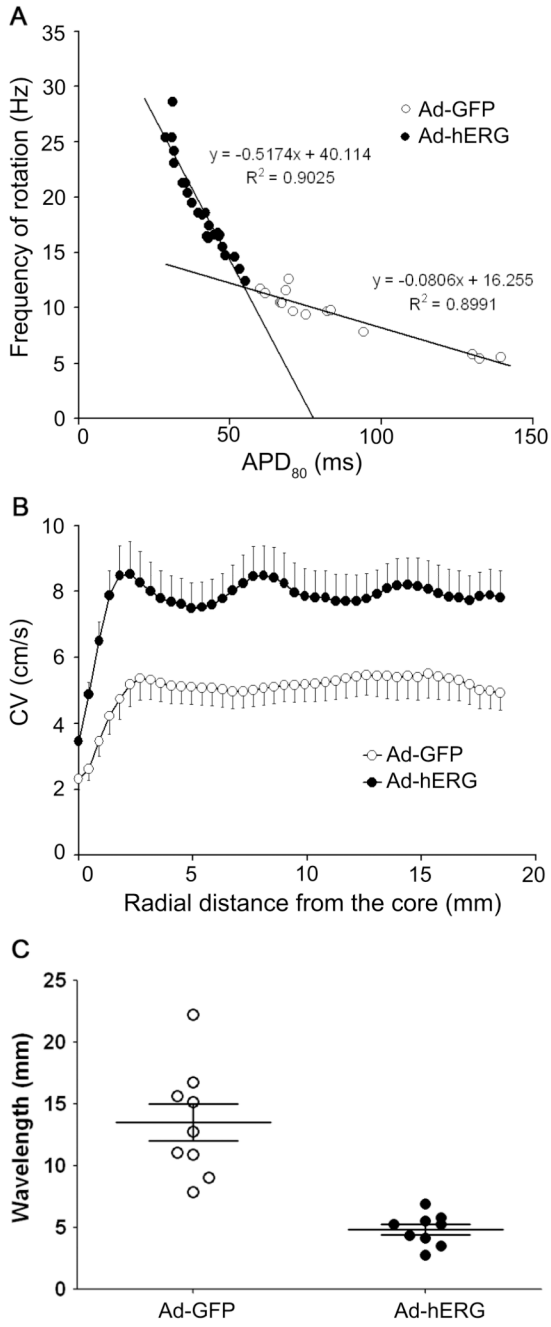

Figure 5.

Effects of hERG overexpression on mean APD, CV and WL during sustained reentry in Ad-GFP (open symbols) and Ad-hERG monolayers (closed symbols). **A**. Rotation frequency as a function of APD_{80}. The regression lines relating frequency to APD is significantly steeper in Ad-hERG monolayers than control ($p<0.05$). Solid lines indicate linear regressions. **B**. CV as a function of distance from the center of rotation (core). CV is significantly higher in Ad-hERG than Ad-GFP infected monolayers at all distance from the core during reentry ($p<0.05$). **C**. Wavelength of reentry. The difference is statistically significant between Ad-GFP and Ad-hERG ($p<0.05$).

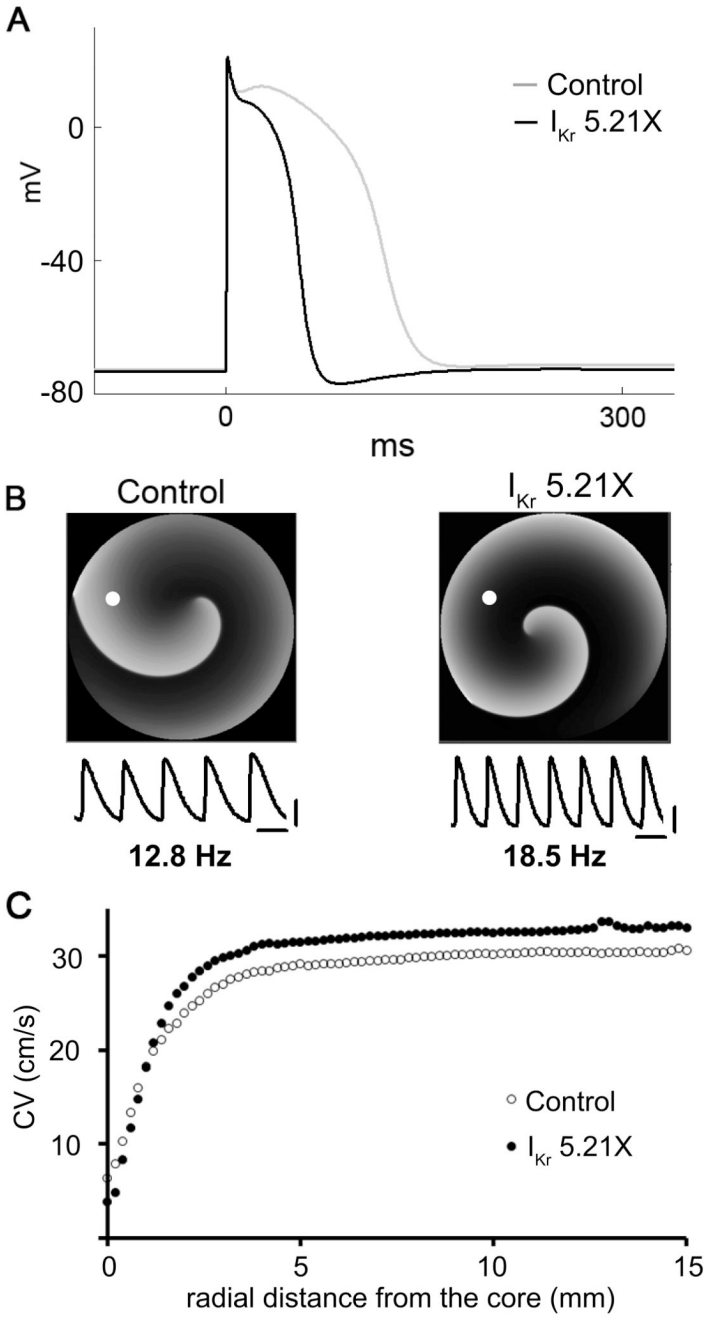

Figure 6.

Numerical simulation using a neonatal rat ventricular myocyte (NRVM) model. **A**. Simulated action potentials in control and I_{Kr} 5.21X. Note progressive APD abbreviation and transient hyperpolarization after the action potential in I_{Kr} 5.21X. **B**. Top, snapshots of 2D simulations of reentry in control and I_{Kr} 5.21X in a NRVM model. Reentry frequency is 12.8 Hz in control (left) and 18.5 Hz in I_{Kr} 5.21X (right). Bottom, action potentials calculated at the position of the white dot on each reentry snapshot. Scale bars, horizontal = 50 ms; vertical = 20 mV. **C**. CV as a function of distance from the center of rotation (core).

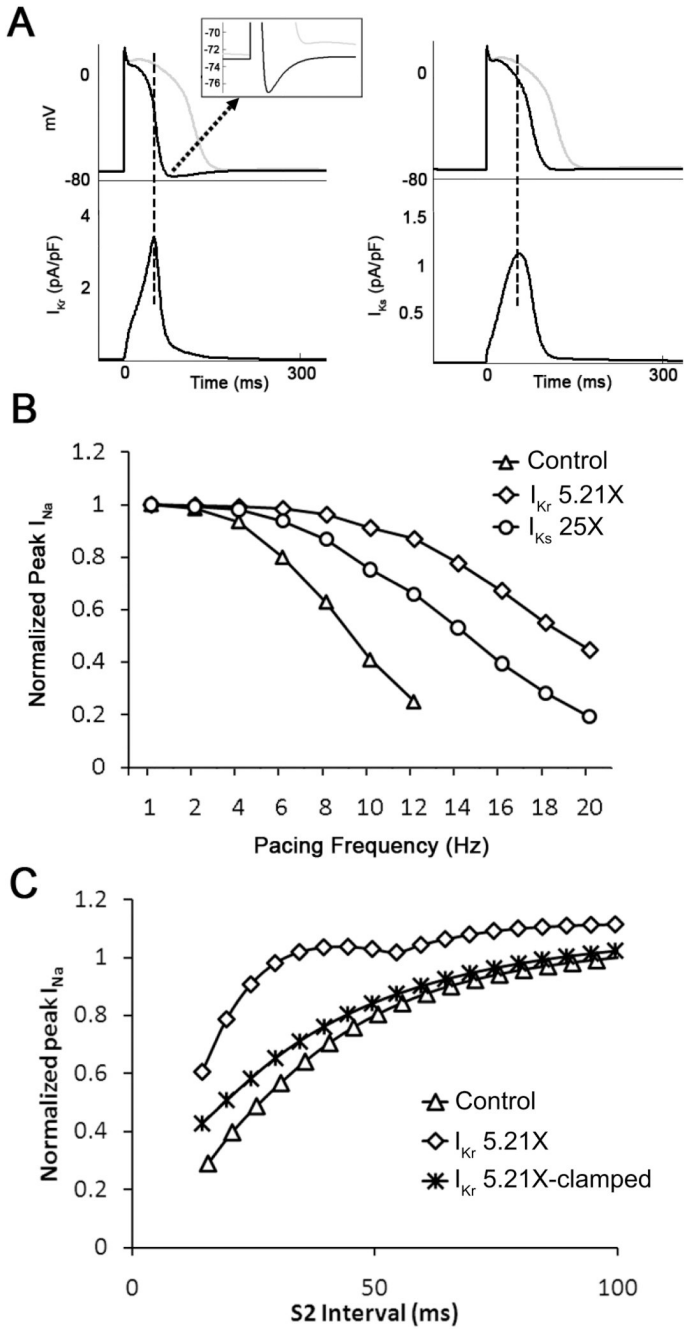

Figure 7.

Simulations demonstrate different consequences of I_{Kr} vs I_{Ks} upregulation on membrane potential and I_{Na} availability. **A**. Superimposed single cell action potentials obtained in control (gray traces), I_{Kr} 5.21X (black traces, left) and I_{Ks} 25X (black traces, right). The APD shortening effect of increasing I_{Kr} was greater than I_{Ks}. In addition, transient hyperpolarization occurred only for I_{Kr} upregulation. Inset, expanded voltage versus time trace emphasizes I_{Kr}-induced transient hyperpolarization. **B**. I_{Na} peak density as a function of pacing frequency in control, I_{Kr} 5.21X and I_{Ks} 25X increase. For control and increased I_{Ks}, the magnitude of I_{Na} decreased monotonically with increasing pacing frequency. For I_{Kr} upregulation, I_{Na} increased at pacing frequencies between 10 and 20 Hz indicating increased

cell excitability. **C**. A single cell I_{Kr} 5.21X model was paced at 2 Hz for 10 sec (S1) followed by a premature S2 stimulus. At shorter S2 intervals, significantly higher I_{Na} was observed as compared to control. This increased I_{Na} availability was suppressed when the minimum diastolic potential (MDP) of the cell was clamped to −70 mV.

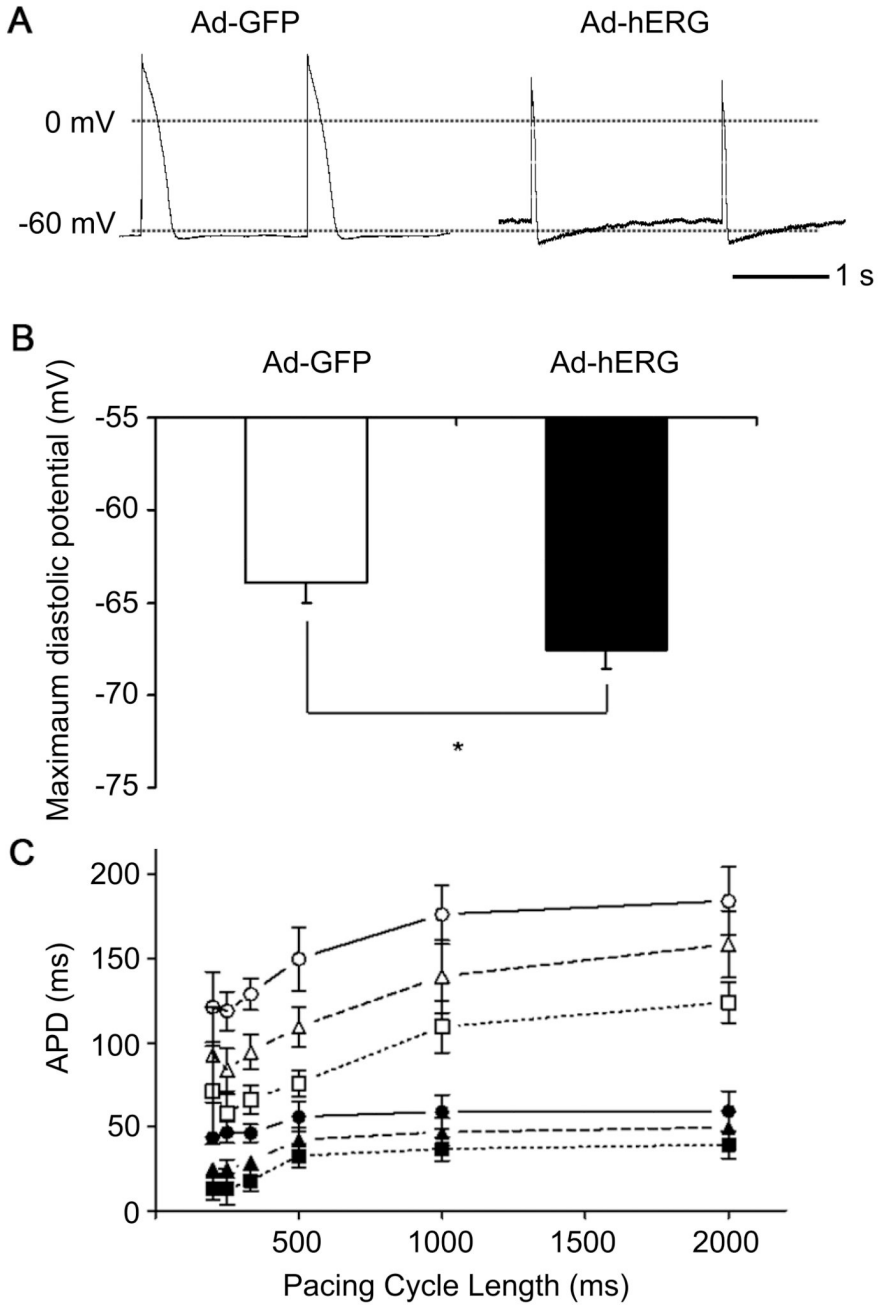

Figure 8.

I_{Kr} overexpression produces transient hyperpolarization after each action potential in isolated NRVMs. **A**. Representative current clamp recordings. Left: action potential in myocyte infected with Ad-GFP; Right: action potential in myocyte infected with Ad-hERG. **B**. Maximal diastolic potential in Ad-hERG and Ad-GFP cells. C. Frequency dependence of APD_{30} (squares), APD_{50} (triangles) and APD_{80} (circles) in myocytes infected with Ad-GFP (filled symbols) or Ad-hERG (open symbols. Student's paired t test.